

Self-consistent theory of the thermal softening and instability of simple crystals

M. J. W. Dodgson,^{a,b} V. B. Geshkenbein,^{a,c} M. V. Feigel'man,^c and G. Blatter^a

^a *Theoretische Physik, ETH-Hönggerberg, CH-8093 Zürich, Switzerland*

^b *Theory of Condensed Matter Group, Cavendish Laboratory, Cambridge, CB3 0HE, UK*

^c *L. D. Landau Institute for Theoretical Physics, 117940 Moscow, Russia*

(July 5, 2000)

We consider the thermal softening of crystals due to anharmonicity. Self-consistent methods find a maximum temperature for a stable crystal, which gives an upper bound to the melting temperature. Previous workers have shown that the self-consistent harmonic approximation (SCHA) gives misleading results for the thermal stability of crystals. The reason is that the most important diagrams in the perturbation expansion around harmonic theory are not included in the SCHA. An alternative approach is to solve a self-consistent Dyson equation (SCA) for a selection of diagrams, the simplest being a (3+4)-SCA. However, this gives an unsatisfactory comparison to numerical results on the thermal and quantum melting of two-dimensional (2D) Coulomb-interacting particles (equivalent to vortex-lattice melting in two and three dimensions). We derive an improved self-consistent method, the two-vertex-SCHA, which gives much better agreement to the simulations. Our method allows for accurate calculation of the thermal softening of the shear modulus for 2D crystals and for the lattice of vortex-lines in type-II superconductors.

PACS numbers: 63.70.+h, 64.70.Dv, 62.20.Dc, 74.60.Ec, 74.60.Ge

I. INTRODUCTION

It was realized long ago on theoretical grounds that most melting transitions should be first order,¹ although exceptions include the possibility of defect-mediated melting in two-dimensional (2D) crystals² and the mean-field transition between the superconducting vortex lattice and the normal state in type-II superconductors.³ As with most first-order transitions, there is no good simple theory of melting to compare with our theoretical understanding of many continuous phase transitions: A first-order transition occurs when the free energy of one phase as a function of temperature crosses the free energy of another phase (see Fig. 1). These two phases are qualitatively different and generally demand theoretical treatments with distinct approximations, such that a detailed comparison of free energies is not possible. The solid-liquid transition is a prime example of this problem. We can treat the solid phase well within elasticity theory, but this is not a useful description of the liquid.

A common approach to this problem is to concentrate on the solid phase and calculate its stability limit⁴ (a complementary method is to treat the liquid, e.g. within density functional theory,⁵ and find the lowest temperature for the liquid phase to exist). A plausible mechanism for the crystal instability comes from anharmonic effects that may soften the lattice when thermal fluctuations are large. To this end one can develop a self-consistent harmonic approximation (SCHA),^{4,6} where an effective harmonic theory is used that better approximates the true anharmonic system for finite thermal fluctuations. We can then identify the limit to a self-consistent solution with the instability temperature of the solid. While it is unclear whether or not the instability point T_u is close

to the melting temperature T_m , it does give an upper bound (see Section III), and represents the first step to understanding the possible mechanisms of melting for a given system.

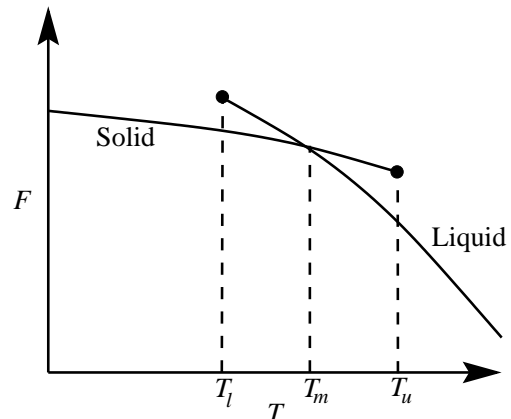


FIG. 1. Schematic diagram of the free energy as a function of temperature for a first-order phase transition. The thermodynamic phase is the one of lowest free energy, and the possibility of a (meta-)stable solution of a phase exists beyond the temperature of the transition.

An example of this hunt for the anharmonic instability point occurred several years ago in the context of 2D melting. An early SCHA calculation by Platzman and Fukuyama⁷ for a 2D electron system found a dramatic stiffening of the Wigner crystal as a function of temperature, and the anharmonic instability point was reached well above the dislocation-mediated melting temperature. Later, Fisher considered anharmonic corrections from a perturbation expansion around the harmonic

theory, and could show that the lowest-order temperature correction to the shear modulus was downwards.⁸ The opposite result of the SCHA calculation comes from the fact that it misses contributions from odd anharmonicities. A series of papers by Lozovik and coworkers⁹ emphasized this fact, and developed an alternative self-consistent procedure from the Dyson equation for the two lowest order diagrams of the expansion. This alternative method was named the (3+4)-self consistent approximation (SCA). (The SCA is distinguished from the SCHA in that self-consistency comes from the Dyson resummation of a set of skeletal diagrams in the perturbation theory, rather than by using an effective harmonic theory to take averages over the true Hamiltonian.) An important result of Lozovik's work was that for long-range interactions in 2D, the anharmonic instability point lies below the dislocation mediated melting temperature, implying a first-order rather than continuous transition.

Our own interest in the melting problem originates in studies of the vortex system in high- T_c superconductors (see Ref. 10 for a review.) There is excellent experimental evidence for a first-order melting transition of the vortex lattice in clean crystals of $\text{Bi}_2\text{Sr}_2\text{CaCu}_2\text{O}_8$ (BSCCO)¹¹ and $\text{YBa}_2\text{Cu}_3\text{O}_{7-\delta}$ (YBCO),^{12,13} with a latent heat and magnetization step consistent with our theoretical models of the vortex system.¹⁴ However, the detailed understanding of where and why this transition takes place has so far relied on numerical simulations.^{15–20} With this in mind, we have tried to apply the above analytic extensions to elasticity theory within the London model²¹ to derive the instability point of the vortex crystal. By comparing our results to the numerical simulations of Ref. 15 we have found, in agreement with Lozovik, that the SCHA seriously underestimates the thermal softening of the vortex lattice (see Section VI C). However, application of the diagrammatic (3+4)-SCA did not lead to a good quantitative comparison, and so we have developed an improved self-consistent method that includes all diagrams in the (3+4)-SCA and the SCHA. Because the improved method uses an effective harmonic theory, but is equivalent to the Dyson equation for all two-vertex diagrams, we call it the two-vertex-SCHA. The successful comparison of this new method to numerical results for the vortex lattice forms the main result of this paper.

The article is structured as follows. We first define the harmonic approximation for a generalized crystal. Then in Section III we describe the self-consistent harmonic approximation and its justification within a variational approach. In Section IV we review the perturbation expansion about the harmonic approximation, look at the diagrams corresponding to the SCHA and see why this approximation can give such misleading results. The alternative (3+4)-SCA of Lozovik *et al.* is also introduced, and we discuss the advantages and disadvantages over the SCHA. After learning the diagrammatic details of these self-consistent approximations, in Section V we introduce our improved self-consistent method, the two-vertex-SCHA, that includes all diagrams in both the

SCHA, (3+4)-SCA and more, while keeping some of the simplicity in treatment of the SCHA. Finally in Section VI we apply this improved method to some physical problems. First we consider the thermal melting in two dimensions of the “one-component plasma” (with $\ln(R)$ interactions) and the Wigner crystal (with $1/R$ interactions). In contrast to the (3+4)-SCA, our results from the two-vertex-SCHA leave open the possibility of dislocation-mediated melting. We also calculate the quantum melting of 2D bosons, equivalent to thermal melting of vortex lines. We find a significant thermal softening of the vortex lattice, which could be responsible for the observed peak effect²² in critical current close to the melting transition in YBCO.

II. REVIEW OF HARMONIC THEORY

We consider a classical d -dimensional crystal at finite temperature, where the particle positions make small fluctuations $\{\mathbf{u}_\mu\}$ about their equilibrium sites $\{\mathbf{R}_\mu\}$. All thermodynamic properties are controlled by the partition function,

$$Z = \int \prod_\mu d^d u_\mu e^{-H[\mathbf{u}_\mu]/T}, \quad (1)$$

where the Hamiltonian $H[\mathbf{u}_\mu]$ gives the energy increase from the ground state for a given configuration of displacements.²³ We work in Fourier space (which diagonalizes a harmonic Hamiltonian), and define,

$$\mathbf{u}_\mathbf{k} = \frac{1}{n} \sum_{\mathbf{R}_\mu} \mathbf{u}_\mu e^{-i\mathbf{k} \cdot \mathbf{R}_\mu}, \quad (2)$$

where n is the particle density. The inverse transform is an integral over the Brillouin zone,

$$\mathbf{u}_\mu = \int_{\text{BZ}} \frac{d^d k}{(2\pi)^d} \mathbf{u}_\mathbf{k} e^{i\mathbf{k} \cdot \mathbf{R}_\mu}. \quad (3)$$

In the harmonic approximation (HA) we expand the Hamiltonian to second order in displacements,

$$H[\mathbf{u}_\mu] = H_2[\mathbf{u}_\mu] + \mathcal{O}(u^3), \quad (4)$$

with

$$H_2[\mathbf{u}_\mu] = \frac{1}{2n^2} \sum_\mu \sum_\nu \Phi_0^{\alpha\beta}(\mathbf{R}_\mu - \mathbf{R}_\nu) u_\mu^\alpha u_\nu^\beta, \quad (5)$$

$$= \frac{1}{2} \int_{\text{BZ}} \frac{d^d k}{(2\pi)^d} \Phi_0^{\alpha\beta}(\mathbf{k}) u_\mathbf{k}^\alpha u_{-\mathbf{k}}^\beta. \quad (6)$$

The elastic matrix is defined by

$$\Phi_0^{\alpha\beta}(\mathbf{k}) = L^d \left. \frac{\delta^2 H}{\delta u_\mathbf{k}^\alpha \delta u_{-\mathbf{k}}^\beta} \right|_{u=0}. \quad (7)$$

Here L^d is the total volume, which determines the discretization of k -space. We define the harmonic Green's function as the inverse of the elastic matrix, $G_0^{\alpha\beta}(\mathbf{k}) = (\Phi_0^{-1})^{\alpha\beta}(\mathbf{k})$.

The HA, being a quadratic theory, is completely solvable, with the size of fluctuations given by the equipartition theorem. The harmonic propagator is the thermal average,

$$\begin{aligned} \langle u_{\mathbf{k}_1}^\alpha u_{\mathbf{k}_2}^\beta \rangle_0 &= Z_0^{-1} \int \Pi_{\mathbf{k}'} d^d u_{\mathbf{k}'} u_{\mathbf{k}_1}^\alpha u_{\mathbf{k}_2}^\beta e^{-H_2[\mathbf{u}_{\mathbf{k}'}]/T} \\ &= T \delta^d(\mathbf{k}_1 + \mathbf{k}_2) G_0^{\alpha\beta}(\mathbf{k}_1), \end{aligned} \quad (8)$$

where Z_0 is the partition function for the harmonic Hamiltonian H_2 . For dimensions $d > 2$ a useful measure of the fluctuations is the mean-square displacement of each particle (in 2D we need to be careful about divergences at long wavelengths, see Appendix A). This is just the integral over \mathbf{k} of the propagator,

$$\langle u^2 \rangle_0 = \langle u^\alpha(\mathbf{R}) u^\alpha(\mathbf{R}) \rangle_0 = T \int_{\text{BZ}} \frac{d^d k}{(2\pi)^d} G_0^{\alpha\alpha}(\mathbf{k}). \quad (9)$$

III. THE SELF-CONSISTENT HARMONIC APPROXIMATION

From Eq. (9) we see how the mean displacements increase with temperature. At some stage the anharmonic corrections to Eq. (4) become important. One way to treat these anharmonic effects is to take the quadratic form as a trial Hamiltonian,

$$H_t[\mathbf{u}_{\mathbf{k}}] = \frac{1}{2} \int_{\text{BZ}} \frac{d^d k}{(2\pi)^d} \Phi_t^{\alpha\beta}(\mathbf{k}) u_{\mathbf{k}}^\alpha u_{-\mathbf{k}}^\beta, \quad (10)$$

with the elastic matrix as a set of variational parameters. We can then use the general inequality²⁴ for the free energy $F = -T \ln Z$,

$$F \leq F_t + \langle H - H_t \rangle_t, \quad (11)$$

so that for a given trial Hamiltonian we get the best approximation to the free energy by minimizing the right hand side. It is straightforward to show that for the quadratic form this minimization is satisfied by the effective elastic matrix,

$$\Phi_t^{\alpha\beta}(\mathbf{k}) = L^d \left\langle \frac{\delta^2 H}{\delta u_{\mathbf{k}}^\alpha \delta u_{-\mathbf{k}}^\beta} \right\rangle_t, \quad (12)$$

where the average is over the distribution defined by the trial Hamiltonian (10) at the given temperature. This must be solved self-consistently, which defines the SCHA.

Let us consider the general case of a system of particles with pairwise interactions,

$$H = \frac{1}{2} \sum_{\mu \neq \nu} V(\mathbf{R}_\mu + \mathbf{u}_\mu - \mathbf{R}_\nu - \mathbf{u}_\nu), \quad (13)$$

where \mathbf{R}_μ are the ideal crystal positions with nearest neighbor separation a . Eq. (12) then becomes,

$$\Phi_t^{\alpha\beta}(\mathbf{k}) = n \sum_{\mu \neq 0} (1 - \cos \mathbf{k} \cdot \mathbf{R}_\mu) \left\langle \frac{\partial^2 V}{\partial r^\alpha \partial r^\beta} \right\rangle_{\mathbf{r}=\mathbf{R}_\mu + \mathbf{u}_\mu - \mathbf{u}_0} \Big|_t. \quad (14)$$

This average over the second derivative of the potential is conveniently written in terms of the displacement fluctuations by Fourier transforming the interaction potential,

$$\begin{aligned} &\left\langle \frac{\partial^2 V}{\partial r^\alpha \partial r^\beta} \right\rangle_{\mathbf{r}=\mathbf{R}_\mu + \mathbf{u}_\mu - \mathbf{u}_0} \Big|_t \\ &= - \int \frac{d^d q}{(2\pi)^d} q^\alpha q^\beta V(q) e^{i\mathbf{q} \cdot \mathbf{R}_\mu} e^{-\frac{1}{2} q^\alpha q^\beta \langle (u_\mu^\alpha - u_0^\alpha)(u_\mu^\beta - u_0^\beta) \rangle}. \end{aligned} \quad (15)$$

Because the fields in a harmonic potential will have Gaussian fluctuations, we have used the property $\langle e^{ikx} \rangle = e^{-\frac{1}{2} k^2 \langle x^2 \rangle}$ for a Gaussian distributed variable x . Although not necessary for calculations, the formalism simplifies greatly if we can make the approximation that $\langle (u_\mu^\alpha - u_0^\alpha)(u_\mu^\beta - u_0^\beta) \rangle = (2/d) \delta_{\alpha\beta} \langle u^2 \rangle$, which means ignoring correlations between the fluctuations of different particle positions. In this case we find,

$$\begin{aligned} \Phi_t^{\alpha\beta}(\mathbf{k}) &= n^2 \sum_{\mathbf{Q}_\mu} (\mathbf{Q}_\mu + \mathbf{k})^\alpha (\mathbf{Q}_\mu + \mathbf{k})^\beta f(|\mathbf{Q}_\mu + \mathbf{k}|) \\ &\quad - Q_\mu^\alpha Q_\mu^\beta f(Q_\mu), \end{aligned} \quad (16)$$

where \mathbf{Q}_μ are the reciprocal lattice vectors, and $f(q) = V(q) e^{-q^2 \langle u^2 \rangle / d}$. The fluctuations $\langle u^2 \rangle$ are calculated from the equipartition theorem (9) but with the Green's function given as the inverse of the effective elastic matrix. Thus within this homogeneous approximation, we have turned the problem of finding $\Phi_t^{\alpha\beta}(\mathbf{k})$ for all \mathbf{k} to a self-consistent equation for a single parameter, $\langle u^2 \rangle$. From (16) it is clear that at large $\langle u^2 \rangle$ the elastic matrix will be suppressed from the zero temperature limit, which in turn increases $\langle u^2 \rangle$ above the harmonic expectation. It is this feature which drives an anharmonic instability of the crystal phase at a certain temperature.

The SCHA in the ‘‘independent fluctuations’’ approximation has an interesting feature for the case of Coulomb interactions ($1/r$ in three dimensions, $\ln r$ in two dimensions etc.). By definition the Laplacian of a Coulomb interaction is zero, and one can show that the renormalized interaction, and therefore the effective elastic matrix, is a non-perturbative function of $\langle u^2 \rangle$. This is shown explicitly for the case of logarithmic interactions in two dimensions in Appendix B. For the 2D case, the single particle fluctuations diverge (see Appendix A) even at low temperatures where the shear modulus remains non-zero.² However, the shear modulus

$\mu_t = \lim_{k_y \rightarrow 0} [\Phi_t^{xx}(k_y)/k_y^2]$ is dominated by the nearest-neighbor fluctuations $\langle u^2 \rangle_{nn} = \frac{1}{2} \langle |\mathbf{u}(\mathbf{R}_\mu) - \mathbf{u}(\mathbf{R}_{\mu+1})|^2 \rangle$; the formula for $\mu_t(\langle u^2 \rangle_{nn})$ is given in Section VIA and shown in the inset of Fig. 2. This allows us to illustrate the SCHa in its simplest form. For this 2D Coulomb system we can approximate the equipartition result as $\langle u^2 \rangle_{nn} \sim T/\mu_t$ (i.e. we ignore compression modes, and assume no dispersion). The two equations relating $\langle u^2 \rangle_{nn}$ and μ_t can then be solved graphically for any temperature as in Fig. 2, and the maximum value of $\langle u^2 \rangle_{nn}$ for a stable self-consistent solution is easily found. In this case we find the large value of $\langle u^2 \rangle_{nn}/a^2 \approx (0.34)^2$ at T_u .

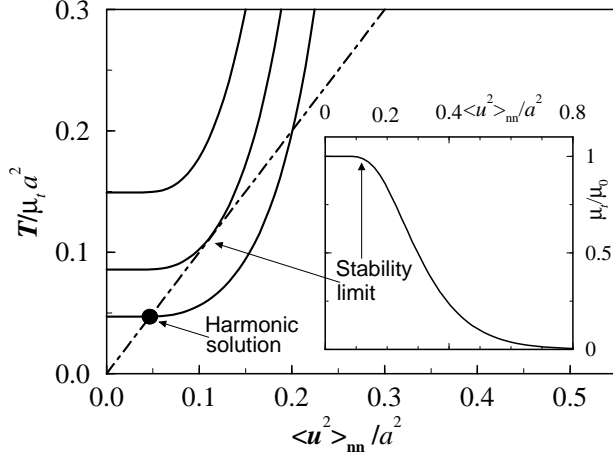


FIG. 2. Illustration of the SCHa for a 2D Coulomb system (see Section VIA). The inset shows the shear modulus μ_t of the 2D Coulomb lattice as a function of nearest-neighbor displacements $\langle u^2 \rangle_{nn}$, as given in Eq. (39). We show graphical solutions to the equipartition result, $\langle u^2 \rangle_{nn} \sim T/\mu_t$ for three different temperatures. At high temperatures there are no self-consistent solutions. Note the non-perturbative form of μ_t at small fluctuations: The curve cannot be approximated by a power series in $\langle u^2 \rangle_{nn}$. In fact, further investigation of the diagrammatics shows that this result severely underestimates the thermal softening of the lattice.

The following argument indicates that this instability point in the SCHa is a rigorous upper bound on the true stability limit of the crystal phase. If there is no solution to the SCHa then by definition there is no stationary value of the RHS of Eq. (11), which implies that this RHS is an unbounded function of trial parameters. Because of the inequality, there can be no finite free energy F , and no equilibrium phase corresponding to the exact Hamiltonian $H[\mathbf{u}_\mathbf{k}]$. Therefore the only possible equilibrium phase is one without a well-defined mapping from particle positions to reference lattice points. In this case the Fourier transforms $\mathbf{u}_\mathbf{k}$ are not the relevant variables of the system, and the liquid phase is still allowed.

Unfortunately, it is known that the SCHa is not always a reliable approximation, and we referred in the introduction to an example where it drastically underestimates the thermal softening of the lattice.⁷ To under-

stand why this is so we must consider which diagrams the SCHa represents in a perturbation expansion around the harmonic limit, and this is done in Section IV B.

IV. PERTURBATION THEORY BEYOND THE HARMONIC APPROXIMATION

We now consider the standard perturbation expansion about the HA.²⁵ The exact partition function is,

$$Z = \int \prod_{\mathbf{k}} d^d u_{\mathbf{k}} e^{-\{H_2[\mathbf{u}_\mathbf{k}] + H'[\mathbf{u}_\mathbf{k}]\}/T}, \quad (17)$$

where $H'[\mathbf{u}_\mathbf{k}] = H[\mathbf{u}_\mathbf{k}] - H_2[\mathbf{u}_\mathbf{k}]$. As usual we expand the exponential in H' ,

$$Z = Z_0 + \sum_{n=1}^{\infty} \frac{(-1)^n}{n!} \int \prod_{\mathbf{k}} d^d u_{\mathbf{k}} \left(\frac{H'[\mathbf{u}_\mathbf{k}]}{T} \right)^n e^{-H_2[\mathbf{u}_\mathbf{k}]/T}. \quad (18)$$

With the same expansion, the propagator is,

$$\begin{aligned} \langle u_{\mathbf{k}}^\alpha u_{-\mathbf{k}}^\beta \rangle &= Z^{-1} \int \prod_{\mathbf{k}'} d^d u_{\mathbf{k}'} u_{\mathbf{k}}^\alpha u_{-\mathbf{k}}^\beta e^{-\{H_2[\mathbf{u}_{\mathbf{k}'}] + H'[\mathbf{u}_{\mathbf{k}'}]\}/T} \\ &= \langle u_{\mathbf{k}}^\alpha u_{-\mathbf{k}}^\beta \rangle_0 \\ &+ \sum_{n=1}^{\infty} \frac{(-1)^n}{n!} \left\langle \left\| u_{\mathbf{k}}^\alpha u_{-\mathbf{k}}^\beta \left(\frac{H'[\mathbf{u}_{\mathbf{k}'}}{T} \right)^n \right\| \right\rangle_{c, G_0}. \end{aligned} \quad (19)$$

The brackets $\langle \|\dots\| \rangle_{c, G_0}$ denote a cumulant average in the HA, that is, using Wick's theorem the u fields must be paired up to give harmonic Green's functions, G_0 , and all terms with disconnected pairings are ignored, as these cancel exactly with the expansion of the partition function Z in the denominator. To establish the terms in this series at each order in T , we need to separate each order in u of the Hamiltonian,

$$H'[\mathbf{u}_\mathbf{k}] = H_3[\mathbf{u}_\mathbf{k}] + H_4[\mathbf{u}_\mathbf{k}] + H_5[\mathbf{u}_\mathbf{k}] + \dots \quad (20)$$

where $H_m[\mathbf{u}_\mathbf{k}]$ contains all terms of order u^m , and will lead to a vertex in the diagrammatic expansion with m legs. Explicitly,

$$H_m = \frac{1}{m!} \int_{BZ} \prod_{i=1}^m \frac{d^d k_i}{(2\pi)^d} A^{\lambda_1 \dots \lambda_m}(\mathbf{k}_1, \dots, \mathbf{k}_m) u_{\mathbf{k}_1}^{\lambda_1} \dots u_{\mathbf{k}_m}^{\lambda_m}. \quad (21)$$

The crystal symmetry of the ground state lattice implies that the interaction tensor conserves pseudomomentum,

$$\begin{aligned} A^{\lambda_1 \dots \lambda_m}(\mathbf{k}_1, \dots, \mathbf{k}_m) &\equiv (L^d)^m \left. \frac{\delta^m H}{\delta u_{\mathbf{k}_1}^{\lambda_1} \dots \delta u_{\mathbf{k}_m}^{\lambda_m}} \right|_{u=0} \\ &= \Phi^{\lambda_1 \dots \lambda_m}(\mathbf{k}_1, \dots, \mathbf{k}_{m-1}) \Delta^d(\mathbf{k}_1 + \dots, \mathbf{k}_m), \end{aligned} \quad (22)$$

where $\Delta^d(\mathbf{k}) = \sum_{\mathbf{Q}_\mu} \delta^d(\mathbf{k} + \mathbf{Q}_\mu)$. The important point is that in the HA the expectation of the propagator $\langle u_{\mathbf{k}} u_{-\mathbf{k}} \rangle_0$ is proportional to T , so that the average value of H_m is of order $T^{\frac{m}{2}}$. We can write the perturbation expansion as,

$$\langle u_{\mathbf{k}}^\alpha u_{-\mathbf{k}}^\beta \rangle = \langle u_{\mathbf{k}}^\alpha u_{-\mathbf{k}}^\beta \rangle_0 + \sum_{n=1}^{\infty} \frac{(-1)^n}{n!} \left\langle \left\| u_{\mathbf{k}}^\alpha u_{-\mathbf{k}}^\beta \left(\sum_{m=3}^{\infty} \frac{H_m}{T} \right)^n \right\| \right\rangle_{c, G_0}, \quad (23)$$

and then take all possible pairings using Wick's theorem. We can represent this series in diagrams and the terms to order T^3 are shown in Fig. 3. The order of each diagram (in T) is counted by adding up the number of lines, and subtracting the number of vertices. Notice that to order T^2 , only H_3 and H_4 contribute, while to order T^3 we also have diagrams including H_5 and H_6 . This is a general rule: the terms H_{2m} and H_{2m-1} first appear to order T^m .

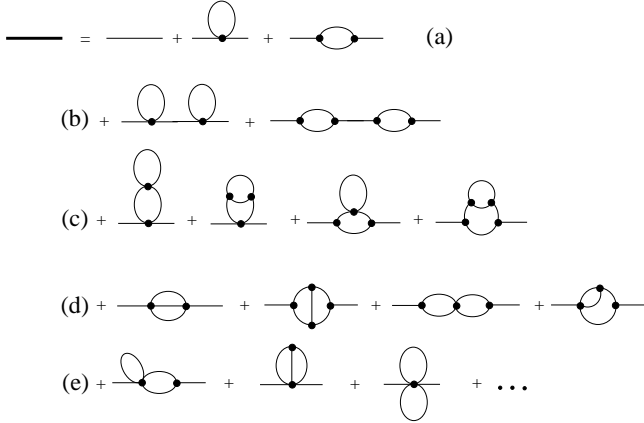


FIG. 3. The diagrammatic expansion of the propagator as described in the text, to order T^3 . We have drawn the diagrams in four groups. Group (a) represents the expansion to order T^2 , which only involves third and fourth order vertices. The remaining groups are all of order T^3 . Group (b) shows the reducible diagrams that are trivial to resum (see text). Group (c) shows the irreducible diagrams to this order that can still be generated by a self-consistent resummation of the lowest order diagrams. Group (d) shows the diagrams that involve only third and fourth order vertices, yet are topologically new to this order. Group (e) shows the first diagrams that include fifth and sixth order vertices.

We now make a resummation that allows us to express the full propagator G in terms of the harmonic propagator G_0 and a self energy Σ . Note that, because we do not include disconnected diagrams, each $u_{\mathbf{k}}$ in (23) must join with a $u_{\mathbf{k}'}$ in H' when using Wick's theorem. This means we can rewrite (23) in the form,

$$\langle u_{\mathbf{k}}^\alpha u_{-\mathbf{k}}^\beta \rangle = \langle u_{\mathbf{k}}^\alpha u_{-\mathbf{k}}^\beta \rangle_0 + \langle u_{\mathbf{k}}^\alpha u_{-\mathbf{k}}^{\lambda_1} \rangle_0 \langle u_{\mathbf{k}}^{\lambda_2} u_{-\mathbf{k}}^\beta \rangle_0 \quad (24)$$

$$\times \sum_{n=1}^{\infty} \frac{(-1)^n}{n!} \left\langle \left\| \frac{\delta^2}{\delta u_{-\mathbf{k}}^{\lambda_1} \delta u_{\mathbf{k}}^{\lambda_2}} \left(\sum_{m=3}^{\infty} \frac{H_m}{T} \right)^n \right\| \right\rangle_{c, G_0}.$$

Inspection of Fig. 3 shows that many possible terms will be trivial “copies” of lower order terms. These are the reducible diagrams, for instance group (b) in Fig. 3, which have the property that when we group all of the reducible diagrams corresponding to a given irreducible diagram, they form a resumable series. We can write this in the compact form

$$G^{\alpha\beta}(\mathbf{k}) = G_0^{\alpha\beta}(\mathbf{k}) + G_0^{\alpha\lambda_1}(\mathbf{k}) \Sigma^{\lambda_1\lambda_2}(\mathbf{k}) G^{\lambda_2\beta}(\mathbf{k}), \quad (25)$$

with the self energy defined as,

$$\Sigma^{\lambda_1\lambda_2}(\mathbf{k}) = T L^d \sum_{n=1}^{\infty} \frac{(-1)^n}{n!} \left\langle \left\| \frac{\delta^2}{\delta u_{-\mathbf{k}}^{\lambda_1} \delta u_{\mathbf{k}}^{\lambda_2}} \left(\frac{H'}{T} \right)^n \right\| \right\rangle_{i, G_0}, \quad (26)$$

The subscript i in the average tells us to only include irreducible contributions, that is, any term which can be separated by cutting just one leg should be ignored, as it is already included in the full Green's function on the RHS of (25). A further resummation is possible by evaluating the RHS of (26) with respect to the renormalized, rather than the harmonic, Green's function. The functional form of the self energy will then depend self-consistently on G ,

$$\Sigma^{\lambda_1\lambda_2}(\mathbf{k}, G) = \quad (27)$$

$$T L^d \sum_{n=1}^{\infty} \frac{(-1)^n}{n!} \left\langle \left\| \frac{\delta^2}{\delta u_{-\mathbf{k}}^{\lambda_1} \delta u_{\mathbf{k}}^{\lambda_2}} \left(\frac{H'}{T} \right)^n \right\| \right\rangle_{s, G},$$

where the subscript s tells us only to include “skeletal” diagrams in the average. We define a skeletal diagram as one that has not already been included in the resummations of lower order diagrams by using the full Green's functions. For instance the diagrams of group (c) in Fig. 3 must be ignored, as they are included when we evaluate the self-energy contribution from group (a) with the renormalized propagator. After these resummations we have a Dyson-type equation, which must be solved self-consistently for G ,

$$(G^{-1})^{\alpha\beta}(\mathbf{k}) = (G_0^{-1})^{\alpha\beta}(\mathbf{k}) - \Sigma^{\alpha\beta}(\mathbf{k}, G). \quad (28)$$

Note that this inverse propagator is exactly the response function $\Phi^{\alpha\beta}(\mathbf{k})$ of the fluctuating crystal for an external force. This is demonstrated in Appendix C.

A. The (3+4)-SCA

Due to the difficulties of calculating all possible diagrams in the perturbation expansion, one looks for approximate resummations. A simple example is to only take the lowest order skeletal diagrams (group (a) in

$$\begin{aligned} \Phi_t^{\alpha\beta}(\mathbf{k}) = & L^d \left\langle \frac{\delta^2 H}{\delta u_{-\mathbf{k}}^\alpha \delta u_{\mathbf{k}}^\beta} \right\rangle_t \\ & - \frac{L^d}{T} \left[\left\langle \frac{\delta H}{\delta u_{-\mathbf{k}}^\alpha} \frac{\delta H}{\delta u_{\mathbf{k}}^\beta} \right\rangle_t \right. \\ & \left. - \left\langle u_{-\mathbf{k}}^{\lambda_1} u_{\mathbf{k}}^{\lambda_2} \right\rangle_t \left\langle \frac{\delta^2 H}{\delta u_{-\mathbf{k}}^\alpha \delta u_{\mathbf{k}}^{\lambda_1}} \right\rangle_t \left\langle \frac{\delta^2 H}{\delta u_{-\mathbf{k}}^{\lambda_2} \delta u_{\mathbf{k}}^\beta} \right\rangle_t \right]. \end{aligned} \quad (34)$$

We call this equation the “two-vertex-SCHA”. The extra terms look rather like a fluctuation contribution to the elasticity, but we should remember that it is simply the two-vertex part of the Dyson series, and there will in principle be further corrections with higher numbers of vertices. The diagrammatic representation of the two-vertex-SCHA is shown in Fig. 6. This scheme now incorporates the diagrams from the SCHA and the (3+4)-SCA along with more terms not included in these last two approaches. For instance, it includes nine of the thirteen diagrams for the propagator at order T^3 , see Fig. 3. It also has the feature of the SCHA that one only needs to calculate averages of derivatives of the full Hamiltonian, and not any diagrams explicitly.

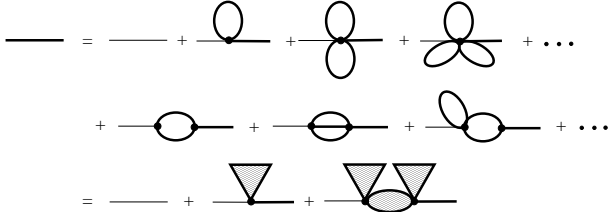


FIG. 6. The two-vertex-SCHA described in diagrams. This approximation includes nine of the thirteen diagrams to order T^3 in Fig. 3. This is equivalent to the self-consistent solution of Eq. (34), so that the diagrams do not need to be explicitly calculated.

VI. PHYSICAL REALIZATIONS

A. The 2D Coulomb system

The 2D Coulomb system, also called the one-component plasma, consists of particles interacting with a pairwise, repulsive logarithmic potential,

$$V(R) = -v \ln(R/\xi). \quad (35)$$

It has been studied in the past partly because of some special mathematical properties²⁷ (the system is exactly soluble at one particular temperature $T = v/2$ in the liquid phase). Numerical simulations^{28–30} have found evidence for a weak first order transition at $T_m \approx 0.007v$. Physically, this system is of interest as it is applicable to a thin superconducting film with field-induced vortices which interact logarithmically³¹ up to a screening length $\Lambda = \lambda^2/d$ where d is the thickness of the film and λ is the

bulk penetration depth, typically of order 1000 Å. Such films were predicted to undergo a 2D melting transition of the vortex lattice well below the zero-field transition temperature.^{32,33} (A similar scenario takes place in layered superconductors at high fields, see Ref. 10.)

The ground state of the 2D Coulomb model is a triangular lattice, with nearest-neighbor spacing $a = (2/n\sqrt{3})^{1/2}$. This lattice has a shear modulus of

$$\mu_0 = \lim_{k_y \rightarrow 0} [\Phi_0^{xx}(k_y)/k_y^2] = \frac{nv}{8} \quad (36)$$

(this result was known over thirty years ago³⁵) and a diverging compression modulus at large wavelengths,

$$\lambda_0(k) = \Phi_0^{xx}(k_x)/k_x^2 \approx 2\pi v n^2/k^2. \quad (37)$$

In Refs. 32 and 33 it was presumed that the melting transition would be of the continuous Kosterlitz-Thouless-Halperin-Nelson-Young (KTHNY) type^{34,2} with a dislocation-unbinding mechanism, which is predicted to occur at

$$T_{\text{KTHNY}} = \mu \frac{a^2}{4\pi} = A(T) \frac{v}{16\sqrt{3}\pi} \approx 0.011 A(T) v \quad (38)$$

with $A < 1$ the renormalization constant for the shear modulus at finite temperature, $\mu = \mu_0 A(T)$. However, this is not consistent with the first-order result of simulations.^{28–30} One possible reason for this discrepancy is that regular fluctuations in an anharmonic potential, such as we considered in the last section, can destabilize the lattice before singular fluctuations such as free dislocations are generated. Therefore in this section we consider the anharmonic softening and instability of the 2D Coulomb lattice, and compare to the predictions of the KTHNY theory. We calculate μ within the SCHA. We also find the first order correction in temperature to the shear modulus using perturbation theory, by calculating the diagrams of group (a) in Fig. 3. This shows that the SCHA greatly underestimates the thermal softening. We then present our results for μ from the (3+4)-SCA and the two-vertex SCHA and compare to the KTHNY universal value of $\mu = 4\pi T_{\text{KTHNY}}/a^2$.

The SCHA for the 2D Coulomb system was briefly looked at in Ref. 27. In fact, the SCHA with “independent fluctuations” has some nice features for this system due to the Laplacian of the interaction being zero. In Appendix B we derive the non-perturbative form of the elastic moduli as a function of $\sigma_{\mu 0} = \frac{1}{2} \langle |\mathbf{u}(\mathbf{R}_\mu) - \mathbf{u}(0)|^2 \rangle$, which leads to the result for the shear modulus,

$$\mu_t = \mu_0 \sum_{\mathbf{R}_\mu} \left(1 - \frac{R_\mu^2}{2\sigma_{\mu 0}} \right) e^{-R_\mu^2/2\sigma_{\mu 0}} \quad (39)$$

$$\approx \mu_0 + 6\mu_0 \left(1 - \frac{a^2}{2\langle u^2 \rangle_{\text{nn}}} \right) e^{-a^2/2\langle u^2 \rangle_{\text{nn}}}. \quad (40)$$

This formula is shown in the inset of Fig. 2 (the nearest-neighbor approximation here is extremely accurate). The

non-perturbative feature (the extreme flatness at small $\langle u^2 \rangle_{\text{nn}}$) will be lost when we include the correlations in fluctuations between different particles. In fact, we have found that the SCHA predicts an initial stiffening of lattice with small fluctuations, which we understand to be an incorrect result due to the neglect of diagrams with odd vertices.

Inspection of Eq. (28) shows the correct temperature expansion of the change in shear modulus to be,

$$\mu = \mu_0 - \lim_{k \rightarrow 0} \Sigma^{xx}(k_y, G)/k_y^2. \quad (41)$$

We can find the first correction to the shear modulus to order T by evaluating the bare self-energy contributions in the diagrams of Fig. 4. Formulas for the (3+4) self-energies for a system with pairwise interactions are given in Appendix D. We have numerically evaluated these formulas for the 2D Coulomb system, and our results for the transverse $\Sigma^T = \Sigma^{yy}(k_x)$ and longitudinal $\Sigma^L = \Sigma^{xx}(k_x)$ parts taking $G = G_0$ are shown in Fig. 7. The large wavelength limits are found to go as,

$$\Sigma_3^T(k) \approx (14T/a^2)k^2 \quad \Sigma_4^T(k) \approx -(10T/a^2)k^2 \quad (42)$$

$$\Sigma_3^L(k) \approx 98T/a^4 \quad \Sigma_4^L(k) \approx (10T/a^2)k^2 \quad (43)$$

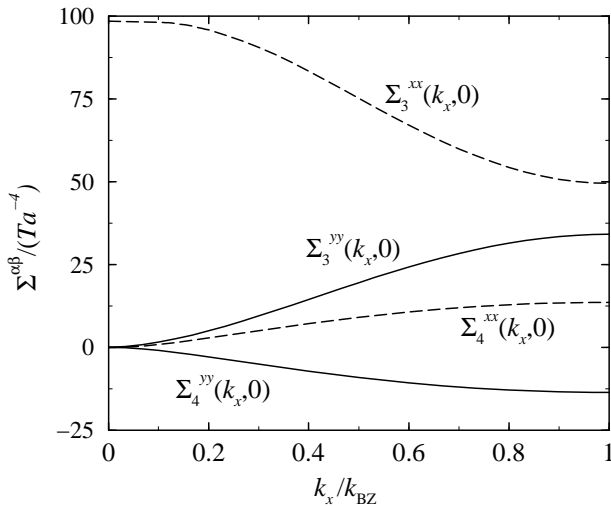


FIG. 7. Contributions to the transverse and longitudinal self energy from the skeletal diagrams of Fig. 4, as given by Eqs. (D3) and (D4), for logarithmic pairwise interactions in 2D.

From Eqs. (41) and (42) the shear modulus at low temperatures will be given by

$$\mu \approx \mu_0 \left(1 - 28 \frac{T}{v} \right), \quad (44)$$

so that within first-order perturbation theory, μ is about 80% of its zero temperature value at the numerically observed transition at $T_m \approx 0.007v$. The large wavelength

limit of the longitudinal part of the self energy in (43) is a constant, so that the compressional modes are also softened to first order in temperature,

$$\lambda(k) \approx \frac{2\pi n^2 v}{k^2} \left(1 - 12 \frac{T}{v} \right). \quad (45)$$

This thermal softening of the long-wavelength compression energy (a special feature of the 2D Coulomb system) might seem to contradict the physically intuitive expectation that the compressibility is fixed by the bare charge of the system. A full understanding of this result will be discussed in a future paper, but it is due to the non-linear relation between changes in the density and the longitudinal displacements, $\delta n = n \nabla \cdot \mathbf{u} + \mathcal{O}(u^2)$.

We can go beyond the lowest order in T using the (3+4) self energy by iterating the equation of Fig. 4 until a stable solution is found within this (3+4)-SCA. We have also found numerical solutions within the two-vertex-SCHA of Section V. Details for calculating the effective elastic moduli of Eq. (34) for pairwise interactions are given in Appendix E. As we have shown in Section V, this approximation gives identical results to lowest order in T as the (3+4)-SCA. However, we find important deviations at larger temperatures. In Fig. 8 the results for μ as a function of temperature from both methods are shown. The shear modulus was recently measured in the same system with Langevin-dynamics simulations,³⁶ and we find good agreement between the measured temperature dependence (the circles in Fig. 8) and the two-vertex-SCHA calculation. Notice that the instability point from the (3+4)-SCA is below the numerically measured melting temperature of $T_m \approx 0.007v$, while the upper limit to solutions of the two-vertex-SCHA is slightly above this temperature.

In Fig. 8 we also compare to the predictions of the KTHNY theory of 2D melting. As described above, this theory predicts a universal value of the shear modulus at the dislocation-unbinding transition, $\mu = 4\pi T/a^2$, shown as the dot-dashed line in Fig. 8. The fact that the two-vertex-SCHA result crosses this value tells us that the results at temperatures above this value are unphysical, as the crystal is unstable to free dislocations (if the (3+4)-SCA were correct, it would practically rule out the KTHNY mechanism for this system). Therefore the crossing of the universal jump and the two-vertex-SCHA result is an upper bound to a melting transition and we find $T_u = 0.0072v$ (the effect of thermally generated dislocation pairs will push μ , and the melting temperature, down further). The fact that at melting the shear modulus is so close to the KTHNY universal value tells us that dislocation-pairs (not included in our analysis) as well as anharmonicities both play an important role in the physics of the melting transition. Whether the weak first-order nature seen in simulations is correct, or a numerical artifact, remains unclear.

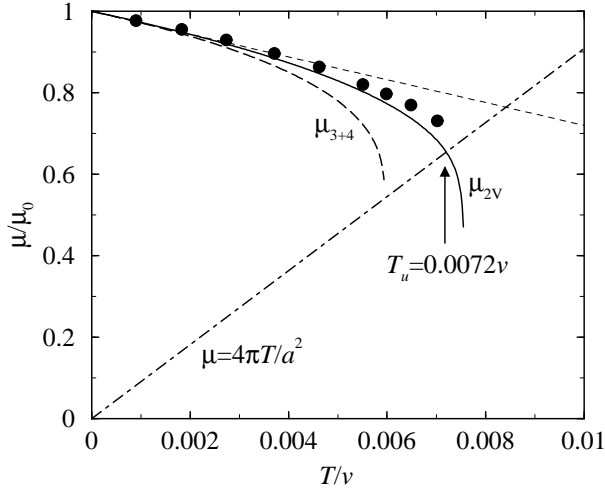


FIG. 8. The shear modulus of the 2D Coulomb crystal as a function of temperature as calculated to first-order in Eq. (44) (short dashed line), and within the (3+4)-SCA (long dashed line) and the two-vertex-SCHA (full line). At higher orders in T we see that the two-vertex-SCHA predicts less softening than the (3+4)-SCA, and a correspondingly higher instability temperature, T_u . The circles are the measured values of μ from numerical simulations taken from Ref. 36. They agree well with the two-vertex-SCHA curve. The dot-dashed line follows the universal jump prediction of the KTHNY transition, $\mu = 4\pi T/a^2$. Below this line the lattice is unstable to free dislocations.

B. Classical electrons in two dimensions

It is experimentally feasible to confine electrons to a flat surface in various systems, such that they are free to move in only two dimensions. In particular, for electrons trapped on the surface of liquid helium by an applied electric potential, a classical melting transition from a 2D “Wigner crystal” to a liquid state has been observed.³⁷ The elastic properties of the 2D Wigner crystal are well studied,^{38,39} and Platzman and Fukuyama⁷ considered the effect of thermal fluctuations using the SCHA, reporting a dramatic stiffening of the lattice with temperature. Using the perturbation expansion of Section IV, Fisher⁸ showed this to be incorrect, as the first order term in T gives a downward correction to μ . Lozovik *et al.* have applied their (3+4)-SCA to this problem,⁹ and stated that an anharmonic instability is reached below the KTHNY temperature. However, the discrepancy in Section VIA for logarithmic interactions between the (3+4)-SCA and our two-vertex-SCHA motivates us to reconsider the 2D Wigner crystal.

Electrons interact with a repulsive pairwise potential,

$$V(R) = \frac{e^2}{R}, \quad (46)$$

where e is the electron’s charge. The ground state is a triangular lattice, spacing a , and at finite temperatures all

properties depend on the dimensionless ratio $T/(e^2 a^{-1})$. In the literature the parameter $\Gamma = \sqrt{\pi} n^{1/2} e^2 / T$ is more often used. When calculating the elastic matrix, care must be taken to split the interaction to long- and short-range parts, and treat them separately as in the Ewald technique.³⁹ Then the zero-temperature shear modulus is found to be,

$$\mu_0 = 0.2450645 e^2 n^{3/2}, \quad (47)$$

and the compression modulus diverges at small k (as for the Coulomb crystal but with a different power) as

$$\lambda_0(k) = \frac{2\pi e^2 n^2}{k}. \quad (48)$$

Repeating the perturbation theory of Section IV we find the first-order correction to the shear modulus to be,

$$\mu \approx \mu_0 \left(1 - 15 \frac{T}{e^2 n^{1/2}} \right), \quad (49)$$

in agreement with Ref. 8. This correction again comes from a negative contribution from $\Sigma_3^T(G_0)$ and a positive, but smaller in magnitude, contribution from $\Sigma_4^T(G_0)$. We have also confirmed that the SCHA gives an incorrect stiffening of μ with increasing temperature.

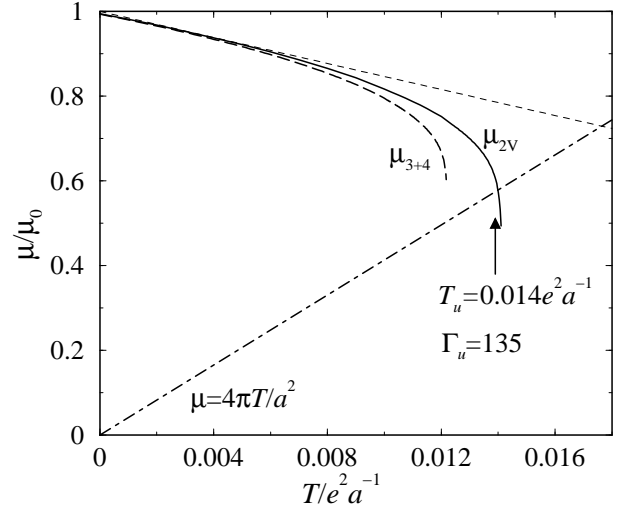


FIG. 9. The shear modulus of the 2D Wigner crystal as a function of temperature. We show the first-order correction of Ref. 8 (short dashed line), and our results for the (3+4)-SCA (long dashed line) and the two-vertex-SCHA (full line). The results are qualitatively the same as for the Coulomb crystal in Fig. 8 with the two-vertex-SCHA result crossing the KTHNY universal jump line (dot-dashed line).

In Fig. 9 we plot our results for the shear modulus $\mu(T)$ from the (3+4)-SCA and the two-vertex-SCHA. The resulting picture is very similar to that for logarithmically interacting particles in Fig. 8. Our instability point for the (3+4)-SCA of $\Gamma_u^{3+4} \approx 155$ is close to the quoted value from Lozovik *et al.* of $\Gamma_u^{3+4} = 140$. The two-vertex-SCHA is again more stable, and together with the

KTHNY condition on the minimum allowed $\mu(T)$ gives $\Gamma_u^{\text{TV}} \approx 135$. This is close to the experimental melting temperature of $\Gamma_m = 127 \pm 5$,^{37,40} valid over a range of experimental densities. Also, numerical simulations have found a melting transition in the range from $\Gamma_m^{\text{sim}} \approx 90$ (Ref. 41) to $\Gamma_m^{\text{sim}} \approx 125$ (Ref. 42 and 43) to $\Gamma_m^{\text{sim}} \approx 159$ (Ref. 44). (It is not clear why there is such disagreement between the numerical results. The rather high melting temperature from the earliest simulation⁴¹ is probably an out of equilibrium artifact; the system was started in the crystal state and heated up.)

C. Quantum melting of 2D bosons and the Bose model of vortex-lattice melting

In the previous sections we have ignored the effect of quantum fluctuations. The uncertainty principle can prevent the formation of a lattice phase if the mass of the particles is sufficiently low. In this section we will consider the effect of quantum fluctuations on a 2D Coulomb lattice of bosons at zero temperature. In the path-integral representation, the action of the boson system in imaginary time is,

$$S = \int_0^{\hbar/T} d\tau \frac{m}{2} \sum_{\mu} \left| \frac{d\mathbf{R}_{\mu}}{d\tau} \right|^2 + \frac{1}{2} \sum_{\mu \neq \nu} V(|\mathbf{R}_{\mu} - \mathbf{R}_{\nu}|), \quad (50)$$

with $V(R)$ given in Eq. (35). The properties of the system are determined by the statistical sum, or partition function, $Z = \text{Tr}_{\mathbf{R}_{\mu}(\tau)} [e^{-S/\hbar}]$. At zero temperature all properties depend only on the unitless de Boer parameter, $\Lambda = (\hbar^2/a^2vm)^{1/2}$, which measures the ratio of zero-point kinetic energy to the interaction energy.

This model maps directly to a 3D classical system at finite temperature, where the world lines of the bosons correspond to fluctuating elastic strings. In fact, the Coulomb interaction between the strings provides a model of the interactions between vortex lines in a type-II superconductor (this fruitful analogy was discovered by Nelson⁴⁵). Thus the path-integral representation of 2D bosons has been studied with the motivation of describing vortex-lattice melting^{15,46} which occurs at finite magnetic fields in high- T_c superconductors.¹⁰ To be specific, the 3D vortex system is obtained by replacing \hbar with T , the time τ with the distance along the field direction z and the mass m with the line elasticity ε_l . (In fact, this model only approximates the 3D interactions of the vortex system. A more correct mapping would be from a boson system with interactions non-local in time.) The strength of the interaction per unit length is determined by the penetration depth λ of the superconductor via the relation $v \rightarrow 2\varepsilon_0$ with $\varepsilon_0 = (\phi_0/4\pi\lambda)^2$ where the quantum of flux is $\phi_0 = hc/2e$. In these units the de Boer parameter is

$$\Lambda = T (a^2 2\varepsilon_0 \varepsilon_l)^{-1/2}. \quad (51)$$

In the numerical simulations^{15,46} a melting transition occurs at $\Lambda \approx 0.062$, above which the system is in a liquid phase. Although it has proved difficult to measure the equilibrium values of the elastic moduli in the same simulations, the value of $\langle u^2 \rangle$ was measured, and shows deviations from a linear dependence on temperature before melting occurs.⁴⁶ In this section we use our self-consistent treatment to find the effect of anharmonicity and the instability point in this system and compare our results to the measured $\langle u^2 \rangle$ in the simulations. We also calculate the quantitative effect of fluctuations on the shear modulus of the vortex crystal.

In the following we use the notation for the classical vortex system, but all results are easily transferred to the 2D quantum system at zero temperature. The generalizations to fluctuating lines of the results of Sections 2–5 are straightforward, where the displacement variables are 2D vectors in 3D \mathbf{k} -space,

$$\mathbf{u}_{\mathbf{k}} = \frac{1}{n} \int dz \sum_{\mathbf{R}_{\mu}} \mathbf{u}_{\mu}(z) e^{-i(\mathbf{k}_{\perp} \cdot \mathbf{R}_{\mu} + k_z z)}. \quad (52)$$

The elastic matrix and the self energy are now functions of k_z as well as the 2D vector \mathbf{k}_{\perp} . Brief details of the (3+4)-SCA and the two-vertex-SCHA are given in Appendix F.

At large wavelengths the transverse elastic matrix is given by $\lim_{k \rightarrow 0} \Phi^T(\mathbf{k}) = c_{66}k_{\perp}^2 + c_{44}k_z^2$ and the longitudinal modes by $\lim_{k \rightarrow 0} \Phi^L(\mathbf{k}) = c_{11}k_{\perp}^2 + c_{44}k_z^2$ where c_{11} , c_{66} and c_{44} are the Voigt notation for the compression, shear and tilt moduli respectively. We can again find the first correction to the shear modulus by evaluating the self energy to lowest order in T . We find that $\Sigma_3^T(k_{\perp}) \approx 3.2(T/a^2a_z)k_{\perp}^2$ and $\Sigma_4^T(k_{\perp}) \approx -2.0(T/a^2a_z)k_{\perp}^2$, where $a_z = a(\varepsilon_l/\varepsilon_0)^{1/2}$. Therefore to lowest order in the de Boer parameter,

$$c_{66} \approx c_{66}^0 (1 - 5.5\Lambda), \quad (53)$$

where the shear modulus without fluctuations is $c_{66}^0 = n\varepsilon_0/4$. The compression modulus at large wavelengths is not renormalized. Note that the ‘‘Hartree’’ self-energy $\Sigma_4(\mathbf{k})$ is independent of the z -component of the wave-vector (see Appendix F), but the contribution $\Sigma_3(\mathbf{k})$ does depend on k_z . For example, for \mathbf{k}_{\perp} at the Brillouin zone we find, $\Sigma_3^{xx}(k_{\perp}^x = k_{\text{BZ}}, k_z) \approx (T/a^4a_z)(8.9 - 2.8a_z^2k_z^2)$, which gives a fluctuation induced stiffening of the tilt modulus,

$$c_{44}(k_{\perp}^x = k_{\text{BZ}}) \approx \frac{\varepsilon_l}{a^2} (1 + 3.9\Lambda). \quad (54)$$

We have made detailed calculations for the two-vertex-SCHA for this model, and the results for the shear modulus as a function of Λ are shown in Fig. 10. It turns out that the effective elastic matrix (see Appendix F)

depends on the full correlations of displacement fluctuations of a given vortex line in the z -direction, and we need to numerically find a self-consistent solution for the function,

$$\begin{aligned} \langle u^2(z) \rangle &\equiv \langle u^\alpha(z) u^\alpha(0) \rangle \\ &= T \int_{-\infty}^{\infty} \frac{dk_z}{2\pi} \int_{\text{BZ}} \frac{d^2 k_\perp}{(2\pi)^2} e^{-ik_z z} (\Phi_t^{-1})^{\alpha\alpha}(\mathbf{k}). \end{aligned} \quad (55)$$

In practise we discretize along the z -direction, making sure that $\langle u^2(z) \rangle$ is smoothly varying.

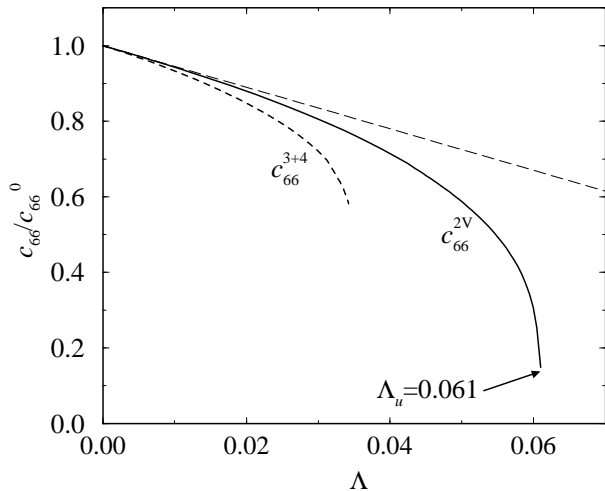


FIG. 10. Shear modulus for 2D bosons with quantum fluctuations, or for the Bose model of the vortex lattice at finite temperature. The long-dashed line is the first-order result (53). The short-dashed line is the result from the (3+4)-SCA, while the full line is the shear modulus calculated in the two-vertex-SCHA. Note that a stable solution is found for much smaller values of the shear modulus than for a two-dimensional system at finite temperature (see Fig. 8).

We again see that the stability limit from the two-vertex-SCHA is higher than that from the (3+4)-SCA. Surprisingly, the crystal maintains a self-consistent solution for a shear modulus which is only 20% of the zero-temperature value. This contrasts with our results for a 2D crystal, and is mainly due to the stiffness of the elastic lines: the average displacements within the equipartition theorem only grow with the inverse square-root of the shear modulus,¹⁰ $\langle u^2 \rangle \propto T/\sqrt{c_{66}c_{44}}$. The result is qualitatively similar to the measured shear modulus in simulations of coupled vortex pancakes in a layered superconductor in Ref. 36. In their somewhat different model of a vortex lattice, a reduction in the shear modulus at melting of about 30% of the zero temperature value was found. Also, we find that the tilt modulus stiffens slightly with the fluctuations, allowing for a still softer shear modulus before instability is reached.

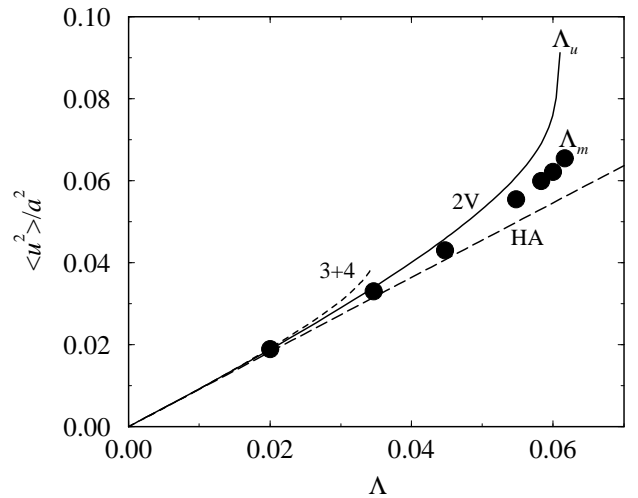


FIG. 11. Comparison of the single-particle fluctuations as measured in Monte Carlo simulations of Ref. 46 and as calculated in this paper. The circles are data from Ref. 46 and the full line is from the two-vertex SCHA, with a stability limit close to the numerical melting. The long dashed line is the harmonic result. The (3+4)-SCA (short-dashed line) becomes unstable well below melting, while the instability point of the SCHA (not shown) overestimates the melting point by a factor two.

In Fig. 11 we compare the mean fluctuation per particle $\langle u^2(0) \rangle = (2\pi)^{-3} \int d^3 k \langle u_{\mathbf{k}}^\alpha u_{-\mathbf{k}}^\alpha \rangle$ with the values measured in simulations (see Fig. 8 of Ref. 46). The simulation results come from fitting a Debye-Waller factor to the measured widths of the crystal structure factor.⁴⁶ The main point is that the instability point predicted by the two-vertex-SCHA, $\Lambda_u = 0.061$ is very close the numerically measured melting point $\Lambda_m = 0.062$. The fact that we find Λ_u slightly below melting means that the two-vertex-SCHA still slightly overestimates the level of softening, and correspondingly there is an increasing discrepancy with the numerical results for $\langle u^2 \rangle$ close to the melting temperature. We should of course remember that the two-vertex-SCHA is only a limited resummation of the perturbation theory. However, our new method clearly gives much superior results compared to the (3+4)-SCA, also shown in the figures, and to the SCHA, which we found to give very little change to the elastic moduli below the numerically found melting and an instability bound over twice the value of Λ_m .

The thermal softening of the shear modulus of the vortex lattice is rarely explicitly calculated in the literature. The measurements from simulations in Ref. 36 agree with Fig. 10 in that this softening is really significant. It may help to explain the peak effect in the critical current seen close to the vortex-lattice melting transition in YBCO.²² The weak collective pinning theory predicts that, for a non-dispersive tilt modulus, the critical current depends on the elastic moduli as $j_c \propto \gamma^2/c_{66}^2 c_{44}$ where γ is a pinning strength parameter.⁴⁷ However, the effect of finite temperature is not only to reduce the shear modu-

lus, but also to smooth the effective pinning landscape over $\langle u^2 \rangle$, thus reducing the pinning force. To see if our results lead to a critical-current peak as a function of temperature requires a careful analysis of the \mathbf{k} dependent elastic moduli (the critical pinning volume depends on long-wavelength distortions but $\langle u^2 \rangle$ comes from integrating over all modes), and we leave this for a future project.

VII. CONCLUSIONS

In this paper we have introduced a new method, the two-vertex-SCHA, to treat the anharmonicity of simple lattices in the presence of thermal, or quantum, fluctuations. The method is based on the diagrammatic expansion about the HA, but takes the form of an extension to the SCHA calculation of effective elastic moduli. By considering two long-range interacting systems at finite temperature, and a system of zero-temperature 2D bosons, we have seen that the two-vertex-SCHA is a significant improvement over previously used self-consistent techniques, the SCHA and the (3+4)-SCA, which respectively under- and overestimated the fluctuation-induced softening. It is the comparison to simulation results that gives us the most confidence in the reliability of the two-vertex-SCHA as a tool for calculating the softening and instability of such simple crystals due to thermal or quantum fluctuations. One should therefore not trust the results of previous treatments of the anharmonic softening of 2D lattices,^{7,9} but use instead the two-vertex-SCHA.

In addition to establishing this new method, we have found important results for the vortex-lattice melting problem, using the Bose model for the finite-temperature

vortex system. We have found a much larger than expected thermal softening of vortex lattice with the shear modulus reducing to 20% of its zero temperature value at the melting transition, which may have important consequences for the pinning properties of the vortex lattice. It should be noted, however, that the real vortex system does not only have interactions within planes of equal height, as in the Bose model. The full London model of vortices corresponds to a 2D Bose system with time-nonlocal interactions.⁴⁸ An investigation to extend the results of the Bose model to the full time-nonlocal case is underway.⁴⁹ Another facet of the vortex system in high- T_c superconductors is the layered nature of the cuprates. For very weak inter-layer coupling, the system can be described by magnetically coupled “pancake” vortices. In a recent paper the two-vertex-SCHA has been used to find the instability line of such a pancake-vortex lattice.⁵⁰ It lies just above the melting line as calculated with a free energy comparison using results from 2D simulations for the pancake-vortex liquid phase. Finally, it would also be interesting to investigate the stability of lattices in the presence of quenched disorder. This is also relevant for the vortex lattice, where pinning disorder exists, and a disorder-induced melting transition occurs as the vortex density, or magnetic field, is increased.⁵¹

ACKNOWLEDGMENTS

We thank Anne van Otterlo, Henrik Nordborg, Alex Koshelev, Boris Ivlev and Valerii Vinokur for useful discussions, and the Swiss National Foundation for financial support. MJWD is supported by an EPSRC Advanced Fellowship AF/99/0725.

APPENDIX A: NEAREST-NEIGHBOR FLUCTUATIONS IN TWO DIMENSIONS

In the SCHA defined by Eq. (14), we have to take averages over the second derivative of the potential between two particles as they fluctuate within the crystal (similar averages are needed in the two-vertex-SCHA, see Appendix E). Within the Gaussian approximation these averages only depend on the mean square, $\sigma_{\mu 0} = \frac{1}{2} \langle |\mathbf{u}(\mathbf{R}_\mu) - \mathbf{u}(0)|^2 \rangle$, which in two dimensions is given by

$$\sigma_{\mu 0} = T \int_{BZ} \frac{d^2 k}{(2\pi)^2} (1 - e^{i\mathbf{k} \cdot \mathbf{R}_\mu}) \left[\frac{1}{\mu k^2} + \frac{1}{\lambda k^2} \right] \approx \frac{T}{\varepsilon_V} \ln(R_\mu/a), \quad (\text{A1})$$

(ε_V is an energy-density scale set by the interaction V). Note that the fluctuations of a single particle, $\langle u^2 \rangle = \lim_{R_\mu \rightarrow \infty} (\sigma_{\mu 0})$ diverges in 2D. We show here that the logarithmic divergence at large distances is not important for the elastic moduli which have dominant contributions from fluctuations at small distances. Consider the difference between the renormalized and the zero temperature elastic matrix

$$\Phi_t^{\alpha\beta}(\mathbf{k}) - \Phi_0^{\alpha\beta}(\mathbf{k}) = n \sum_{\mu \neq 0} (\cos \mathbf{k} \cdot \mathbf{R}_\mu - 1) \int \frac{d^2 q}{(2\pi)^2} q^\alpha q^\beta V(q) e^{i\mathbf{q} \cdot \mathbf{R}_\mu} \left[e^{-\frac{1}{2} q^2 \sigma_{\mu 0}} - 1 \right]. \quad (\text{A2})$$

Now the Fourier transform only has weight at values of $q < 1/R_\mu$, so as long as $\sigma_{\mu 0} \ll R_\mu^2$ we can write $e^{-\frac{1}{2} q^2 \sigma_{\mu 0}} \approx 1 - \frac{1}{2} q^2 \sigma_{\mu 0}$ and,

$$\Phi_t^{\alpha\beta}(\mathbf{k}) - \Phi_0^{\alpha\beta}(\mathbf{k}) \approx n \sum_{\mu \neq 0} (\cos \mathbf{k} \cdot \mathbf{R}_\mu - 1) \frac{1}{2} \sigma_{\mu 0} \nabla^2 \partial_\alpha \partial_\beta V(R_\mu) \quad (\text{A3})$$

Now the R_μ dependence of $\sigma_{\mu 0}$ is logarithmic and weak compared to the short-range variation in $(\cos \mathbf{k} \cdot \mathbf{R}_\mu - 1) \nabla^2 \partial_\alpha \partial_\beta V(R_\mu)$, so short distances will dominate and we are justified to approximate fluctuations by the nearest-neighbor result $\sigma_{\mu 0} \approx \langle u^2 \rangle_{\text{nn}}$. Similar arguments apply for the sums that appear in the two-vertex SCHA. (For logarithmic interactions, $\nabla^2 V(R) = 0$, and the perturbation theory is not helpful. However, for this case the non-perturbative result (39) derived in Appendix B is clearly dominated by the nearest neighbors.)

APPENDIX B: SCHA CALCULATION OF THE FLUCTUATION-RENORMALIZED ELASTICITY FOR LOGARITHMIC INTERACTIONS IN TWO DIMENSIONS

In this appendix we show how to calculate the elastic matrix of a 2D lattice with logarithmic interactions within the SCHA as given by (14) and demonstrate the non-perturbative dependence on the size of fluctuations $\langle u^2 \rangle$. We need the thermal average of the second derivatives of the interaction potential between each pair of particles. Assuming the displacement fluctuations to be Gaussian distributed, this is,

$$\left\langle \frac{\partial^2 V(\mathbf{R}_\mu + \mathbf{u}_\mu - \mathbf{u}_0)}{\partial R^\alpha \partial R^\beta} \right\rangle = \int \frac{d^2 r}{Z} \frac{\partial^2 V(\mathbf{R}_\mu + \mathbf{r})}{\partial r^\alpha \partial r^\beta} \mathcal{P}(\mathbf{r}) = \frac{\partial^2}{\partial R_\mu^\alpha \partial R_\mu^\beta} \langle V(\mathbf{R}_\mu + \mathbf{u}_\mu - \mathbf{u}_0) \rangle \quad (\text{B1})$$

where the derivatives on the RHS do not act on the distribution function,

$$\mathcal{P}(\mathbf{r}) = \exp \left(-\frac{1}{2} r^\alpha (\sigma_{\mu 0}^{-1})^{\alpha\beta} r^\beta \right). \quad (\text{B2})$$

The width of the fluctuations is given by the matrix

$$\sigma_{\mu 0}^{\alpha\beta} = \langle [u^\alpha(\mathbf{R}_\mu) - u^\alpha(\mathbf{0})][u^\beta(\mathbf{R}_\mu) - u^\beta(\mathbf{0})] \rangle, \quad (\text{B3})$$

and $Z = 2\pi [\det(\sigma_{\mu 0}^{\alpha\beta})]^{1/2}$.

We take the isotropic fluctuation approximation, $\sigma_{\mu 0}^{\alpha\beta} = \delta_{\alpha\beta} \sigma_{\mu 0}$, which we find to be good from numerical evaluation of (8) in the HA. In this case, because the potential is circular symmetric, the average will be independent of the angle θ_μ of the ground state position \mathbf{R}_μ , so

$$\begin{aligned} \langle V(R_\mu) \rangle &= \frac{1}{2\pi} \int d\theta_\mu \int \frac{d^2 r}{Z} V(\mathbf{r} + \mathbf{R}_\mu) e^{-\frac{r^2}{2\sigma_{\mu 0}}} \\ &= \frac{1}{2\pi} \int d\theta_\mu \int \frac{d^2 r}{Z} \int_0^{R_\mu} dR \frac{d}{dR} V(\mathbf{r} + \mathbf{R}) e^{-\frac{r^2}{2\sigma_{\mu 0}}} \\ &= \frac{1}{2\pi} \int \frac{d^2 r}{Z} \int_0^{R_\mu} \frac{dR}{R} \int_{\rho < R} d^2 \rho \nabla_\rho^2 V(\mathbf{r} + \rho) e^{-\frac{r^2}{2\sigma_{\mu 0}}}, \end{aligned} \quad (\text{B4})$$

where we have made use of the divergence theorem $\int d\theta_\mu (d/dR) = R^{-1} \oint d\ell \hat{\mathbf{n}} \cdot \nabla = R^{-1} \int_{\rho < R} d^2 \rho \nabla_\rho^2$. We are interested in the case of logarithmic interactions, $V(R) = -v \ln(R/\xi)$, and we use the fact that $\nabla^2 [\ln(R/\xi)] = 2\pi \delta^2(\mathbf{R})$ to give

$$\langle V(R_\mu) \rangle = v \int_0^{R_\mu} \frac{dR}{R} \left[e^{-R^2/2\sigma_{\mu 0}} - 1 \right] = -v \ln(R_\mu/\xi) - v \int_{R_\mu}^\infty \frac{dR}{R} e^{-R^2/2\sigma_{\mu 0}} + \text{const}, \quad (\text{B5})$$

where the integration constant depends on $\sigma_{\mu 0}$ and ξ but not on R_μ . Notice that the correction term to the zero-temperature potential is non-perturbative in the fluctuation $\sigma_{\mu 0}$. The physics of this result is clear: because the 2D-Laplacian of the interaction potential is zero, Gauss' theorem applies and the circular symmetric potential gives the same result as if all of the “mass” was at a point in the center of the circle (the ground state position \mathbf{R}_μ). The non-perturbative correction appears from the exponentially small tail of the distribution which is outside of the radius R_μ . This “shell” does not contribute to the average interaction, so it's weight must be subtracted from the bare interaction. We can easily differentiate the correction term with respect to the lower limit of the integral, to find

$$\left\langle \frac{\partial^2 V(\mathbf{R}_\mu + \mathbf{u}_\mu - \mathbf{u}_0)}{\partial R^\alpha \partial R^\beta} \right\rangle = \frac{\partial^2 V(\mathbf{R}_\mu)}{\partial R_\mu^\alpha \partial R_\mu^\beta} + v \left[\frac{R_\mu^\alpha R_\mu^\beta}{R_\mu^4} \left(2 + \frac{R_\mu^2}{\sigma_{\mu 0}} \right) + \frac{\delta_{\alpha\beta}}{R_\mu^2} \right] e^{-\frac{R_\mu^2}{2\sigma_{\mu 0}}}. \quad (\text{B6})$$

This expression should be inserted into (14) to give the renormalized elastic matrix. It is then straightforward to derive the softening of the shear modulus within the SCHA as given in Eq. (39) and Fig. 2.

APPENDIX C: EQUIVALENCE OF ELASTIC RESPONSE WITH INVERSE PROPAGATOR

We demonstrate in this appendix that the elastic response to an external force is given by the inverse propagator (or Green's function). In the presence of a force \mathbf{f}_μ acting on each particle, the Hamiltonian is changed to,

$$H_f[\mathbf{u}_\mu] = H[\mathbf{u}_\mu] - \sum_\mu \mathbf{f}_\mu \cdot \mathbf{u}_\mu. \quad (\text{C1})$$

The definition of elastic response within the thermally fluctuating region is that the force is given by Hooke's law,

$$f_\mu^\alpha = \sum_\nu \Phi^{\alpha\beta}(\mathbf{R}_\nu - \mathbf{R}_\mu) U_\nu^\beta, \quad (\text{C2})$$

which is valid to lowest order in the mean displacements $U_\nu^\beta = \langle u_\nu^\beta \rangle_f$. The displacements are calculated with straightforward statistical mechanics,

$$U_\nu^\beta = Z_f^{-1} \int \prod_\mu d^2 u_\mu u_\nu^\beta e^{-(H[\mathbf{u}_\lambda] - \sum_\lambda \mathbf{f}_\lambda \cdot \mathbf{u}_\lambda)/T}, \quad (\text{C3})$$

$$= \frac{1}{T} \sum_\mu f_\mu^\alpha \langle u_\nu^\beta u_\mu^\alpha \rangle_{f=0} + \mathcal{O}(f^2). \quad (\text{C4})$$

If we have lattice-translational symmetry, the Fourier transform of this reads as $U_\mathbf{k}^\beta = f_\mathbf{k}^\alpha G^{\alpha\beta}(\mathbf{k})$, where the Green's function is defined by $\langle u_\mathbf{k}^\beta u_{\mathbf{k}'}^\alpha \rangle_{f=0} = T G^{\alpha\beta}(\mathbf{k}) \delta(\mathbf{k} + \mathbf{k}')$, so that the elastic matrix in \mathbf{k} -space is exactly the inverse Green's function,

$$\Phi^{\alpha\beta}(\mathbf{k}) = (G^{-1})^{\alpha\beta}(\mathbf{k}). \quad (\text{C5})$$

Note that this example of the classical fluctuation-dissipation theorem goes beyond the equipartition result, which is only valid for the harmonic approximation. The true elastic response of the fluctuating system is always given by the inverse of the propagator.

If we construct the free energy corresponding to H_f , we will find the result,

$$F_f = F_{f=0} - \frac{1}{2} \int_{\text{BZ}} \frac{d^d k}{(2\pi)^d} (G^{-1})^{\alpha\beta}(\mathbf{k}) U_\mathbf{k}^\alpha U_{-\mathbf{k}}^\beta + \mathcal{O}(f^3). \quad (\text{C6})$$

This is for a system with forces specified. However, one is often interested in the case where a certain displacement is enforced (e.g. when boundary conditions are changed in a numerical simulation). We must then make a Legendre transformation to the relevant thermodynamic potential that depends on a fixed displacement,

$$A(T, [\mathbf{U}_\mu]) = F_f + \sum_\mu f_\mu^\alpha U_\mu^\alpha \quad (\text{C7})$$

$$= F_{f=0} + \frac{1}{2} \int_{\text{BZ}} \frac{d^d k}{(2\pi)^d} (G^{-1})^{\alpha\beta}(\mathbf{k}) U_\mathbf{k}^\alpha U_{-\mathbf{k}}^\beta + \mathcal{O}(U^3). \quad (\text{C8})$$

With this formulation, we see that the elastic matrix may be found as the second derivative of the thermodynamic potential with fixed displacements, $\Phi^{\alpha\beta}(\mathbf{k}) = \partial^2 A / \partial U_\mathbf{k}^\alpha \partial U_{-\mathbf{k}}^\beta \big|_{U=0}$. For example, the $k \rightarrow 0$ shear modulus may be measured as the response to the change in the angle θ determining the boundaries of a finite system as in Ref. 36. As the Hamiltonian will depend on the "displacement" θ , we can differentiate the relevant free energy, $A(T, \theta)$, to give,

$$\mu = L^{-d} \left[\left\langle \frac{\partial^2 H}{\partial \theta^2} \right\rangle_{\theta=0} - \frac{1}{T} \left\langle \left(\frac{\partial H}{\partial \theta} \right)^2 \right\rangle_{\theta=0} + \frac{1}{T} \left\langle \frac{\partial H}{\partial \theta} \right\rangle_{\theta=0}^2 \right] \quad (\text{C9})$$

The important point is that this shear modulus is exactly the same as the shear modulus found from the $k \rightarrow 0$ limit of the inverse of the transverse propagator $\mu = \lim_{k_y \rightarrow 0} [(G^{-1})^{xx}(k_y)/k_y^2]$.

APPENDIX D: THE (3+4)-SCA FOR PAIRWISE INTERACTIONS

In this appendix we show how to explicitly calculate the (3+4) diagrammatic expansion of Fig. 4, for the case of pairwise interactions. For a Hamiltonian of the form (13), the third and fourth rank anharmonic tensors defined by Eqs. (21) and (22) will be given by,

$$\begin{aligned}\Phi^{\lambda_1\lambda_2\lambda_3}(\mathbf{k}_1, \mathbf{k}_2) &= n \sum_{\mu \neq 0} \left(e^{i\mathbf{k}_1 \cdot \mathbf{R}_\mu} + e^{i\mathbf{k}_2 \cdot \mathbf{R}_\mu} + e^{-i(\mathbf{k}_1 + \mathbf{k}_2) \cdot \mathbf{R}_\mu} \right) \frac{\partial^3 V}{\partial R_\mu^{\lambda_1} \partial R_\mu^{\lambda_2} \partial R_\mu^{\lambda_3}} \\ &= in^2 \sum_{\mathbf{Q}_\mu} f_3(\mathbf{Q}_\mu + \mathbf{k}_1) + f_3(\mathbf{Q}_\mu + \mathbf{k}_2) + f_3(\mathbf{Q}_\mu - \mathbf{k}_1 - \mathbf{k}_2),\end{aligned}\quad (\text{D1})$$

and

$$\begin{aligned}\Phi^{\lambda_1\lambda_2\lambda_3\lambda_4}(\mathbf{k}_1, \mathbf{k}_2, \mathbf{k}_3) &= n \sum_{\mu \neq 0} (1 - e^{i\mathbf{k}_1 \cdot \mathbf{R}_\mu}) (1 - e^{i\mathbf{k}_2 \cdot \mathbf{R}_\mu}) (1 - e^{i\mathbf{k}_3 \cdot \mathbf{R}_\mu}) \frac{\partial^4 V}{\partial R_\mu^{\lambda_1} \partial R_\mu^{\lambda_2} \partial R_\mu^{\lambda_3} \partial R_\mu^{\lambda_4}} \\ &= n^2 \sum_{\mathbf{Q}_\mu} f_4(\mathbf{Q}_\mu) - f_4(\mathbf{Q}_\mu - \mathbf{k}_1) - f_4(\mathbf{Q}_\mu - \mathbf{k}_2) - f_4(\mathbf{Q}_\mu - \mathbf{k}_3) - f_4(\mathbf{Q}_\mu - \mathbf{k}_1 - \mathbf{k}_2 - \mathbf{k}_3) \\ &\quad + f_4(\mathbf{Q}_\mu - \mathbf{k}_1 - \mathbf{k}_2) + f_4(\mathbf{Q}_\mu - \mathbf{k}_2 - \mathbf{k}_3) + f_4(\mathbf{Q}_\mu - \mathbf{k}_3 - \mathbf{k}_1),\end{aligned}\quad (\text{D2})$$

with $f_m(\mathbf{Q}) = Q_{\lambda_1} \dots Q_{\lambda_m} V(\mathbf{Q})$. The above Poisson resummations to reciprocal-lattice sums allow for more convenient evaluation, especially in the case of long-ranged interactions. The contribution to the self energy from the “flying-saucer” diagram is,

$$\Sigma_3^{\lambda_1\lambda_2}(\mathbf{k}, G) = \frac{L^d}{2T} \left\langle \frac{\delta^2(H_3^2)}{\delta u_{\mathbf{k}}^{\lambda_1} \delta u_{-\mathbf{k}}^{\lambda_2}} \right\rangle_G = -\frac{T}{2} \int_{\text{BZ}} \frac{d^d k_1}{(2\pi)^d} G^{\lambda_3\lambda_4}(\mathbf{k}_1) G^{\lambda_5\lambda_6}(\mathbf{k} + \mathbf{k}_1) \Phi^{\lambda_1\lambda_3\lambda_5}(\mathbf{k}, \mathbf{k}_1) \Phi^{\lambda_2\lambda_4\lambda_6}(\mathbf{k}, \mathbf{k}_1), \quad (\text{D3})$$

while the contribution from the first, “Hartree”-type diagram is

$$\Sigma_4^{\lambda_1\lambda_2}(\mathbf{k}, G) = -L^d \left\langle \frac{\delta^2 H_4}{\delta u_{\mathbf{k}}^{\lambda_1} \delta u_{-\mathbf{k}}^{\lambda_2}} \right\rangle_G = -\frac{T}{2} \int_{\text{BZ}} \frac{d^d k_1}{(2\pi)^d} G^{\lambda_3\lambda_4}(\mathbf{k}_1) \Phi^{\lambda_1\lambda_2\lambda_3\lambda_4}(\mathbf{k}, -\mathbf{k}, \mathbf{k}_1). \quad (\text{D4})$$

APPENDIX E: THE TWO-VERTEX-SCHA FOR PAIRWISE INTERACTIONS

We now describe the details of the two-vertex-SCHA of Section V for a system with pairwise interactions. Splitting the effective elastic matrix of Eq. (34) term by term we have,

$$\Phi_t^{\alpha\beta}(\mathbf{k}) = \Phi_1^{\alpha\beta}(\mathbf{k}) + \Phi_2^{\alpha\beta}(\mathbf{k}) + \Phi_{2c}^{\alpha\beta}(\mathbf{k}), \quad (\text{E1})$$

with $\Phi_1^{\alpha\beta}(\mathbf{k})$ given by the SCHA formula (14),

$$\Phi_2^{\alpha\beta}(\mathbf{k}) = -\frac{L^d}{T} \left\langle \frac{\delta H}{\delta u_{-\mathbf{k}}^\alpha} \frac{\delta H}{\delta u_{\mathbf{k}}^\beta} \right\rangle = \frac{-1}{4TL^d} \sum_{\substack{\mu \neq \nu \\ \rho \neq \sigma}} (e^{i\mathbf{k} \cdot \mathbf{R}_\mu} - e^{i\mathbf{k} \cdot \mathbf{R}_\nu}) (e^{-i\mathbf{k} \cdot \mathbf{R}_\rho} - e^{-i\mathbf{k} \cdot \mathbf{R}_\sigma}) \left\langle \frac{\partial V}{\partial r^\alpha} \Big|_{\mu-\nu} \frac{\partial V}{\partial r^\beta} \Big|_{\rho-\sigma} \right\rangle, \quad (\text{E2})$$

and,

$$\Phi_{2c}^{\alpha\beta}(\mathbf{k}) = \frac{1}{TL^d} \Phi_1^{\alpha\lambda_1}(\mathbf{k}) \Phi_1^{\beta\lambda_2}(\mathbf{k}) \left\langle u_{-\mathbf{k}}^{\lambda_1} u_{\mathbf{k}}^{\lambda_2} \right\rangle, \quad (\text{E3})$$

where the averages are taken with respect to the effective elastic Hamiltonian. In the independent fluctuation approximation, we can write the entire elastic matrix as a function of $\langle u^2 \rangle$ and T (note that in 2D, although $\langle u^2 \rangle$ diverges, we can take the nearest-neighbor value $\langle u^2 \rangle_{\text{nn}}$ as the sum in (E2) is dominated by short distances),

$$\Phi_2^{\alpha\beta}(\mathbf{k}) = \frac{n^3}{T} \sum_{\mathbf{Q}, \mathbf{Q}'} \left[g_{\mathbf{Q}, \mathbf{Q}'}^{\alpha\beta} - g_{\mathbf{Q}-\mathbf{k}, \mathbf{Q}'}^{\alpha\beta} - g_{\mathbf{Q}, \mathbf{Q}'+\mathbf{k}}^{\alpha\beta} + g_{\mathbf{Q}-\mathbf{k}, \mathbf{Q}'+\mathbf{k}}^{\alpha\beta} \right] + \frac{n^2}{2T} \int \frac{d^d q'}{(2\pi)^d} \sum_{\mathbf{Q}} \left[2h_{\mathbf{Q}-\mathbf{q}', \mathbf{q}'}^{\alpha\beta} - h_{\mathbf{Q}-\mathbf{q}'-\mathbf{k}, \mathbf{q}'}^{\alpha\beta} - h_{\mathbf{Q}-\mathbf{q}'+\mathbf{k}, \mathbf{q}'}^{\alpha\beta} \right], \quad (\text{E4})$$

with

$$g_{\mathbf{q}_1, \mathbf{q}_2}^{\alpha\beta} = q_1^\alpha q_2^\beta V(q_1) V(q_2) e^{-(q_1^2 + q_2^2) \langle u^2 \rangle / d} \left[e^{-\mathbf{q}_1 \cdot \mathbf{q}_2 \langle u^2 \rangle / d} - 1 \right], \quad (\text{E5})$$

and

$$h_{\mathbf{q}_1, \mathbf{q}_2}^{\alpha\beta} = q_1^\alpha q_2^\beta V(q_1) V(q_2) e^{-(q_1^2 + q_2^2) \langle u^2 \rangle / d} \left[e^{-\mathbf{q}_1 \cdot \mathbf{q}_2 \langle u^2 \rangle / d} - 1 \right]^2. \quad (\text{E6})$$

Finally the correction term is given by,

$$\Phi_{2c}^{\alpha\beta}(\mathbf{k}) = \frac{\langle u^2 \rangle}{dnT} \Phi_1^{\alpha\lambda}(\mathbf{k}) \Phi_1^{\beta\lambda}(\mathbf{k}). \quad (\text{E7})$$

To complete the two-vertex-SCHA one must find a self-consistent solution numerically for $\langle u^2 \rangle$ by inserting the effective elastic matrix in the equipartition result (9).

APPENDIX F: MODIFICATIONS FOR INTERACTING ELASTIC STRINGS IN THREE DIMENSIONS

We now outline the generalization of the self-consistent methods to the problem of elastic strings directed along z and interacting within 2D planes of equal z . First, the harmonic energy is given by,

$$H_2 = \frac{1}{2} \int_{\text{BZ}} \frac{d^2 k_\perp}{(2\pi)^2} \int_{-\infty}^{\infty} \frac{dk_z}{2\pi} \left[\Phi_{0, 2D}^{\alpha\beta}(\mathbf{k}_\perp) + \delta_{\alpha\beta} n \epsilon_l k_z^2 \right] u_{\mathbf{k}}^\alpha u_{-\mathbf{k}}^\beta. \quad (\text{F1})$$

The generalization of Eq. (D3) is,

$$\Sigma_3^{\lambda_1 \lambda_2}(\mathbf{k}, G) = -\frac{T}{2} \int_{\text{BZ}} \frac{d^2 k'_\perp}{(2\pi)^2} \int \frac{dk'_z}{2\pi} G^{\lambda_5 \lambda_6}(\mathbf{k} + \mathbf{k}') G^{\lambda_3 \lambda_4}(\mathbf{k}') \Phi_{2D}^{\lambda_1 \lambda_3 \lambda_5}(\mathbf{k}_\perp, \mathbf{k}'_\perp) \Phi_{2D}^{\lambda_2 \lambda_4 \lambda_6}(\mathbf{k}_\perp, \mathbf{k}'_\perp), \quad (\text{F2})$$

and of Eq. (D4) is,

$$\Sigma_4^{\lambda_1 \lambda_2}(\mathbf{k}, G) = -\frac{T}{2} \int_{\text{BZ}} \frac{d^2 k'_\perp}{(2\pi)^2} \int \frac{dk'_z}{2\pi} G^{\lambda_3 \lambda_4}(\mathbf{k}') \Phi_{2D}^{\lambda_1 \lambda_2 \lambda_3 \lambda_4}(\mathbf{k}_\perp, -\mathbf{k}_\perp, \mathbf{k}'_\perp). \quad (\text{F3})$$

The matrices with 2D subscripts are to be calculated for the interactions within a given 2D plane.

For the two-vertex-SCHA we now have to be careful to include the z -correlations in the fluctuation terms, $\langle u^2(z) \rangle = \langle u^\alpha(z) u^\alpha(0) \rangle$. We can again split the effective elastic matrix as in (E1), with Φ_1 being the 2D SCHA elastic modulus plus the single string elasticity, and

$$\begin{aligned} \Phi_2^{\alpha\beta}(\mathbf{k}) &= \frac{n^3}{T} \sum_{\mathbf{Q}, \mathbf{Q}'} \int_{-\infty}^{\infty} dz e^{-ik_z z} \left[g_{\mathbf{Q}, \mathbf{Q}'}^{\alpha\beta}(z) - g_{\mathbf{Q}-\mathbf{k}, \mathbf{Q}'}^{\alpha\beta}(z) - g_{\mathbf{Q}, \mathbf{Q}'+\mathbf{k}}^{\alpha\beta}(z) + g_{\mathbf{Q}-\mathbf{k}, \mathbf{Q}'+\mathbf{k}}^{\alpha\beta}(z) \right] \\ &+ \frac{n^2}{2T} \int \frac{d^2 q'}{(2\pi)^2} \sum_{\mathbf{Q}} \int_{-\infty}^{\infty} dz e^{-ik_z z} \left[2h_{\mathbf{Q}-\mathbf{q}', \mathbf{q}'}^{\alpha\beta}(z) - h_{\mathbf{Q}-\mathbf{q}'-\mathbf{k}, \mathbf{q}'}^{\alpha\beta}(z) - h_{\mathbf{Q}-\mathbf{q}'+\mathbf{k}, \mathbf{q}'}^{\alpha\beta}(z) \right], \end{aligned} \quad (\text{F4})$$

with

$$g_{\mathbf{q}_1, \mathbf{q}_2}^{\alpha\beta}(z) = q_1^\alpha q_2^\beta V(q_1) V(q_2) e^{-\frac{1}{2}(q_1^2 + q_2^2) \langle u^2(0) \rangle} \left[e^{-\frac{1}{2} \mathbf{q}_1 \cdot \mathbf{q}_2 \langle u^2(z) \rangle} - 1 \right], \quad (\text{F5})$$

and

$$h_{\mathbf{q}_1, \mathbf{q}_2}^{\alpha\beta}(z) = q_1^\alpha q_2^\beta V(q_1) V(q_2) e^{-\frac{1}{2}(q_1^2 + q_2^2) \langle u^2(0) \rangle} \left[e^{-\frac{1}{2} \mathbf{q}_1 \cdot \mathbf{q}_2 \langle u^2(z) \rangle} - 1 \right]^2, \quad (\text{F6})$$

where $\langle u^2(z) \rangle$ is defined in Eq. (55). The last, correction term is given by,

$$\Phi_{2c}^{\alpha\beta}(\mathbf{k}) = \frac{1}{2nT} \Phi_{1, 2D}^{\alpha\lambda}(\mathbf{k}_\perp) \Phi_{1, 2D}^{\lambda\beta}(\mathbf{k}_\perp) \int dz e^{-ik_z z} \langle u^2(z) \rangle. \quad (\text{F7})$$

-
- ¹ L. D. Landau, Zh. Eksp. Teor. Fiz. **7**, 19 (1937) [English translation in *Collected papers of L. D. Landau* (Pergamon Press, Oxford, 1965) p. 193].
- ² B. I. Halperin and D. R. Nelson, Phys. Rev. Lett. **41**, 121 (1978); D. R. Nelson and B. I. Halperin, Phys. Rev. B **19**, 2457 (1979).
- ³ A. A. Abrikosov, Sov. Phys. JETP **5**, 1174 (1957).
- ⁴ L. Pietronero, in *Phonons: Theory and Experiments*, edited by P. Brüesch (Springer, Berlin, 1987), Vol. III, Chap. 8.
- ⁵ T. V. Ramakrishnan and M. Youssouf, Phys. Rev. B **19**, 2775 (1979).
- ⁶ H. Kleinert, *Gauge Fields in Condensed Matter* (World Scientific, Singapore, 1989), pp. 913-24.
- ⁷ P. M. Platzman and H. Fukuyama, Phys. Rev. B **10**, 3150 (1974).
- ⁸ D. S. Fisher, Phys. Rev. B **26**, 5009 (1982).
- ⁹ Y. E. Lozovik and V. M. Fartzdinov, Sov. Phys. Solid State **27**, 1458 (1986); Y. E. Lozovik, V. M. Fartzdinov, B. Abdullaev, and S. A. Kucherov, Phys. Lett. **112A**, 61 (1985).
- ¹⁰ G. Blatter, M. V. Feigel'man, V. B. Geshkenbein, A. I. Larkin and V. M. Vinokur, Rev. Mod. Phys. **66**, 1125 (1994).
- ¹¹ E. Zeldov, D. Majer, M. Konczykowski, V. B. Geshkenbein, V. M. Vinokur and H. Shtrikman, Nature (London) **375**, 373 (1995).
- ¹² U. Welp, J. A. Fendrich, W. K. Kwok, G. W. Crabtree, and B. W. Veal, Phys. Rev. Lett. **76**, 4809 (1996).
- ¹³ A. Schilling, R. A. Fisher, N. E. Phillips, U. Welp, D. Dasgupta, W. K. Kwok and G. W. Crabtree, Nature **382**, 791 (1996).
- ¹⁴ M. J. W. Dodgson, V. B. Geshkenbein, H. Nordborg, and G. Blatter, Phys. Rev. Lett. **80**, 837 (1998); Phys. Rev. B **57**, 14498 (1998).
- ¹⁵ H. Nordborg and G. Blatter, Phys. Rev. Lett. **79**, 1925 (1997).
- ¹⁶ X. Hu, S. Miyashita and M. Tachiki, Phys. Rev. Lett. **79**, 3498 (1997).
- ¹⁷ A. E. Koshelev, Phys. Rev. B **56**, 11201 (1997).
- ¹⁸ A. K. Nguyen and A. Sudbø, Phys. Rev. B **57**, 3123 (1998).
- ¹⁹ R. Šášik and D. Stroud, Phys. Rev. Lett. **75**, 2582 (1995).
- ²⁰ J. Hu and A. MacDonald, Phys. Rev. B **56**, 2788 (1997).
- ²¹ E. H. Brandt, J. Low Temp. Phys. **26**, 735 (1977).
- ²² W. K. Kwok, J. A. Fendrich, C. J. van der Beek, G. W. Crabtree, Phys. Rev. Lett. **73**, 2614 (1994); K. Deligiannis, P. A. J. de Groot, M. Oussena, S. Pinfold, R. Langan, R. Gagnon, and L. Taillefer, Phys. Rev. Lett. **79**, 2121 (1997); T. Nishizaki, T. Natio, and N. Kobayashi, Phys. Rev. B **58**, 11169 (1998).
- ²³ We ignore the cohesion energy of the ground state as it does not influence the fluctuations considered in this paper.
- However, if we wanted to calculate the full free energy, e.g. to compare to the liquid state, we would need to include this ground state energy.
- ²⁴ R. P. Feynman and A. R. Hibbs, *Quantum Mechanics and Path Integrals* (McGraw-Hill, New York, 1965), Chap. 11.
- ²⁵ An introduction is given in P. Choquard, *The Anharmonic Crystal* (W.A. Benjamin, New York, 1967).
- ²⁶ P. Minnhagen, Rev. Mod. Phys. **59**, 1001 (1987).
- ²⁷ A. Alastuey and B. Jancovici, J. de Phys. (Paris) **42**, 1 (1981).
- ²⁸ S. W. de Leeuw and J. W. Perram, Physica **113A**, 546 (1982).
- ²⁹ J. M. Caillol, D. Levesque, J. J. Weis, and J. P. Hansen, J. Stat. Phys. **28**, 325 (1982).
- ³⁰ P. Choquard and J. Clerouin, Phys. Rev. Lett. **50**, 2086 (1983).
- ³¹ J. Pearl, Appl. Phys. Lett. **5**, 65 (1964).
- ³² B. A. Huberman and S. Doniach, Phys. Rev. Lett. **43**, 950 (1979).
- ³³ D. S. Fisher, Phys. Rev. B **22**, 1190 (1980).
- ³⁴ J. M. Kosterlitz and D. J. Thouless, J. Phys. C **6**, 1181 (1973).
- ³⁵ A. L. Fetter, P. C. Hohenberg and P. Pincus, Phys. Rev. **147**, 140 (1966).
- ³⁶ Z-X Cai, G. Dubey, and D. O. Welch, Physica C **299**, 91 (1998).
- ³⁷ C. C. Grimes and G. Adams, Phys. Rev. Lett. **42**, 795 (1979).
- ³⁸ R. S. Crandall, Phys. Rev. A **8**, 2136 (1973).
- ³⁹ L. Bonsall and A. A. Maradudin, Phys. Rev. B **15**, 1959 (1977).
- ⁴⁰ G. Deville, J. Low Temp. Phys. **72**, 135 (1988).
- ⁴¹ R. W. Hockney and T. R. Brown, J. Phys. C. **8**, 1813 (1975).
- ⁴² R. C. Gann, S. Chakravarty, and G. V. Chester, Phys. Rev. B **20**, 326 (1979).
- ⁴³ R. H. Morf, Phys. Rev. Lett. **43**, 931 (1979).
- ⁴⁴ V. M. Bedanov, G. V. Gadiyak, and Yu. E. Lozovik, Sov. Phys. JETP **61**, 967 (1985).
- ⁴⁵ D. R. Nelson, Phys. Rev. Lett. **60**, 1973 (1988).
- ⁴⁶ H. Nordborg and G. Blatter, Phys. Rev. B **58**, 14 556 (1998).
- ⁴⁷ A. I. Larkin and Y. N. Ovchinnikov, J. Low Temp. Phys. **34**, 409 (1979).
- ⁴⁸ M. V. Feigel'man, V. B. Geshkenbein, L. B. Ioffe, and A. I. Larkin, Phys. Rev. B **48**, 16641 (1993).
- ⁴⁹ Y. V. Fominov, et al., in preparation.
- ⁵⁰ M. J. W. Dodgson, et al., Phys. Rev. Lett. **84**, 2698 (2000).
- ⁵¹ D. Ertas and D. R. Nelson, Physica C **272**, 79 (1996); T. Giamarchi and P. Le Doussal, Phys. Rev. B **55**, 6577 (1997); A. van Otterlo, R. T. Scalettar and G. T. Zimanyi, Phys. Rev. Lett. **81**, 1497 (1998).